Modeling Gas Transport in the Shallow Subsurface During the ZERT CO_2 Release Test

Curtis M. Oldenburg[1]

Jennifer L. Lewicki[1]

Laura Dobeck[2]

Lee Spangler[2]

[1]Earth Sciences Division 90-1116

Lawrence Berkeley National Laboratory

Berkeley, CA 94720

[2]Department. of Chemistry

Montana State University

Bozeman, MT 59717

November 22, 2008

Abstract

We used the multiphase and multicomponent TOUGH2/EOS7CA model to carry out predictive simulations of CO_2 injection into the shallow subsurface of an agricultural field in Bozeman, Montana. The purpose of the simulations was to inform the choice of CO_2 injection rate and design of monitoring and detection activities for a CO_2 release experiment. The release experiment configuration consists of a long horizontal well (70 m) installed at a depth of approximately 2.5 m into which CO_2 is injected to mimic leakage from a geologic carbon sequestration site through a linear feature such as a fault. We estimated the permeability of the soil and cobble layers present at the site by manual inversion of measurements of soil CO_2 flux from a vertical-well CO_2 release. Based on these estimated permeability values, predictive simulations for the horizontal well showed that CO_2 injection just below the water table creates an effective gas-flow pathway through the saturated zone up to the unsaturated zone. Once in the unsaturated zone, CO_2 spreads out laterally within the cobble layer where liquid saturation is relatively low. CO_2 also migrates upwards into the soil layer through the capillary barrier and seeps out at the ground surface. The simulations predicted a breakthrough time of approximately two days for the 100 kg d^{-1} injection rate, which also produced a flux within the range desired for testing detection and monitoring approaches. The seepage area produced by the model was approximately five meters wide above the horizontal well, compatible with the detection and monitoring methods tested. For a given flow rate, gas-phase diffusion of CO_2 tends to dominate over advection near the ground surface where the CO_2 concentration gradient is large while advection dominates deeper in the system.

Introduction

Large-scale geologic carbon sequestration (GCS) is being considered as an approach to reduce carbon dioxide (CO_2) emissions from the current global carbon-based fossil-fuel energy supply. Associated with GCS is concern that leakage of CO_2 could result in unintended negative environmental and health and safety consequences. Demonstrations by the technical community of the ability to detect, characterize, mitigate, and remediate CO_2 leakage from geologic CO_2 storage sites are needed to satisfy concerns about potential safety and environmental impacts of GCS. While monitoring and detection capabilities are useful at all depths from the reservoir to the near-surface environment, our focus in this work is on the shallow subsurface as the place where health and safety issues are foremost and as the last interface before CO_2 leakage enters the atmosphere.

In order to develop and demonstrate approaches for detection and characterization of surface CO_2 leakage (seepage), the Zero Emissions Research and Technology (ZERT) project team developed the ZERT Release Facility (ZRF) in an agricultural field on the Montana State University campus in Bozeman, Montana. A 100 m-long, approximately 2.5 m deep horizontal well was installed here with a 70 m long central perforated section. This perforated section is divided into six zones by inflatable packers into which CO_2 is injected to emulate leakage from a GCS site through a linear feature such as a fault or fracture. The CO_2 in the shallow subsurface and its efflux at the ground surface (seepage) arising from the injection creates an artificial GCS leakage signal that we observe using various detection and monitoring approaches. This artificial CO_2 source also allows us to study shallow CO_2 transport processes, the understanding of which can be used to design monitoring approaches the exploit one or another process (e.g., advection or diffusion). (In this work, we use the definitions of Oldenburg and Unger (2003) and Oldenburg and Lewicki (2006) who defined

leakage as CO_2 migration away from the storage region, e.g., away from a deep formation that is the reservoir intended to sequester CO_2, and *seepage* as leaking CO_2 that crosses the ground-surface into the atmosphere. By these definitions, CO_2 that has leaked from the GCS site but is still migrating in the subsurface is called leakage while CO_2 migrating across the ground surface is called seepage.)

The purpose of this paper is to present pre-injection (predictive) simulation results of the migration of CO_2 at the ZRF in the summer of 2007. The simulations were carried out to inform the design of the first experiments with respect to considerations such as breakthrough time, magnitude of seepage flux, size and character of the seepage area, and modes of transport (diffusion versus advection) in the shallow system. We also present here a comparison of the predicted fluxes against field measurements as validation of the model predictions. Results of the predictive modeling are presented in four sections organized around the following specific questions: (1) What is the time to breakthrough at the surface as a function of injection rate? (2) What is the expected pattern of CO_2 discharge at the ground surface? (3) What is the temporal variation in seepage due to changes in injection rate? (4) What are the CO_2 transport mechanisms as a function of depth and injection rate?

Motivation and Background

The ubiquity and variability of CO_2 in nature causes enormous challenges for detection of small-scale CO_2 seepage from the shallow subsurface (Oldenburg et al., 2003; Lewicki et al., 2007; Cortis et al., 2008; Leuning et al., 2008). In short, plants and microbes take up and respire CO_2 at variable rates on semi-diurnal to interannual time scales as controlled by variations in biological activity and availability of moisture, nutrients, and energy. The fundamental challenge of surface and near-surface GCS leakage and seepage detection is to discern a signal from within the natural variability of CO_2 in the ecosystem. The purpose of the ZRF is to create a controlled leakage signal within a

functioning ecosystem that can be observed and monitored by multiple teams and methods to test the ability to detect and characterize CO_2 leakage and seepage in the presence of overprints from natural processes.

There is a long history of research using intentional releases of gases for developing methods of detection, monitoring, mitigation, risk assessment, and modeling of gas leaks. Most of the intentional release experiments described in the literature were carried out above-ground, in the environment relevant to industrial plants (e.g., refineries and chemical plants) or to liquefied natural gas (LNG) terminals and transport, and emphasize atmospheric dispersion processes (e.g., Britter, 1989; Hanna and Steinberg, 2001). Activities closest to our objectives include investigations of subsurface transport processes such as those involved in pipeline accidents. Buried pipes are generally much safer than above-ground pipes, but maintaining them and finding leaks when they occur is greatly complicated by the overburden. In research funded by the Gas Research Institute (GRI) aimed at natural gas (CH_4) pipeline leak detection, it was found that thermal, laser, and multispectral remote sensing approaches exhibited limitations, while sampling of soil gas and microbial populations around the leak source allowed detection of an intentional CH_4 release (Wilkey et al., 1992).

The releases modeled in this work involve CO_2 injection below the water table. At the shallow depths of interest, CO_2 will be gaseous and will rise through saturated porous media either as bubble or channel flow depending on the flow rate (Oldenburg and Lewicki, 2006). The processes of injection and buoyant upward flow of CO_2 gas resemble those involved in air sparging (e.g., Ji et al., 1993; Brooks et al., 1999), except that injection is typically deeper and at higher rates in air sparging

than those planned for intentional CO_2 releases such as those at the ZRF designed to mimic low-level CO_2 leakage from GCS sites.. At the injection rates planned for the ZRF, CO_2 is expected to emanate from the slotted pipe and migrate upwards as bubble or channel flow through the saturated cobble region into the vadose zone. In the vadose zone during injection, CO_2 gas will be driven upwards and laterally by pressure driving forces and by gravity (CO_2 is a dense gas relative to air in the pore space).

When modeling flow and transport in the shallow subsurface, hydrologists often rely on soil physics approaches that utilize the Richards equation (e.g., Hillel, 1998). For our purposes in modeling CO_2 flow and transport in the saturated and unsaturated zones, the Richards equation is of little use because it neglects the gas phase which is our primary interest. Although models exist for estimating the velocity of discrete bubbles rising in saturated porous media (e.g., Roosevelt and Corapcioglu, 1998; Corapcioglu, 2004), in general, larger-scale continuum models are needed for addressing the questions posed here involving coupled saturated- and unsaturated-zone flow and transport of gas. The TOUGH2/EOS7CA continuum modeling approach used here models the gas as a second phase in the porous medium with capillary pressure and relative permeability effects.

Methods

We used TOUGH2 (Pruess et al., 1999) along with the research module EOS7CA (Oldenburg and Unger, 2003) for modeling CO_2 transport at the ZRF. TOUGH2/EOS7CA models the Darcy flow and Fickian diffusive transport of five components (water, brine, CO_2, a gas tracer, and air) in gaseous and aqueous phases at near-ambient pressures and temperatures. TOUGH2 is a widely used integral finite-difference multiphase and multicomponent non-isothermal flow and transport simulator that supports numerous equation of state (EOS) modules. The governing equations are

presented in Table 1, and symbols are defined in the nomenclature table. TOUGH2 uses integral equations and solves them implicitly by the integral finite difference method. TOUGH2 uses Newton-Raphson iteration to handle non-linearity, a choice of conjugate gradient sparse matrix solvers to solve the Jacobian matrix at each Newton iteration, and a robust residual-based convergence criterion to ensure convergence of the coupled non-linear equations (Pruess et al., 1999). Note we omit the energy equation in Table 1 because all results in this study were for isothermal conditions. TOUGH2/EOS7CA is designed for near-surface applications where the pseudo component air is present (Oldenburg and Unger, 2003). The use of Henry's Law for modeling solubility restricts EOS7CA to shallow regions (low pressure systems). Other TOUGH2 modules (e.g., ECO2N (Pruess, 2005) and EOS7C (Oldenburg et al., 2004) are available for deep subsurface (high-pressure) systems.

Results

Domain and boundary conditions

The shallow subsurface at the ZRF consists of ~1.2 m of soil overlying a cobble formation with a seasonally variable water table. Data for the soil thickness and water table depth came from shallow wells, soil pits, and borings at the site (Mokwa, 2006). The horizontal injection well consists of a long (100 m) stainless steel pipe installed at a depth of approximately 2.5 m with 15 m (SW end) and 12 m (NE end) sections on each end sloping upward to the surface. The 70-m sub-horizontal section is perforated (slotted) and divided into six sections (five of length 12 m, and one 9 m in length at the SW end) by inflatable packers. The six sections receive CO_2 at independently controlled rates through plastic tubing connected to a flow controller and CO_2 source supply tank by copper tubing. The water table was approximately 1.5 m deep during the test, causing the CO_2 injection to be within the saturated zone. The geometry of the first ZRF experiment was intended to mimic CO_2 leakage

up a linear feature such as a fault or fracture zone. Each of the six packed-off sections received CO_2 at the same flow rate. The long linear geometry lends itself to two-dimensional (2D) modeling in a grid transverse (perpendicular) to the well.

The site characteristics were generalized into 2D model systems consistent with the long horizontal well (2D transverse) and the vertical-well injection (2D radial) geometries. Figure 1 shows the Cartesian 2D transverse model system discretization, boundary conditions, soil layers, and water table location. The well is offset toward the left-hand side to allow the modeling of CO_2 dissolved in groundwater moving from left to right, a process not presented in this paper. The grid is finer around the well at Y = 9.6 m to resolve near-well processes. The radial system (2D radial grid) was used for the vertical-well injection experiment and used the same vertical discretization, soil thickness, and initial liquid saturation as the Cartesian model, but with a radially varying horizontal discretization to resolve the near-well region. The top boundary is held at a constant pressure of 1 bar (10^5 Pa) and constant CO_2 concentration of 380 ppmv (corresponding to CO_2 mass fraction in the aqueous phase equal to 5.76×10^{-4}, which is also the initial and boundary condition throughout the system). All simulations are isothermal at 15 ^{o}C.

The properties of the two layers (soil and cobble) were assigned as shown in Table 1. In the absence of measurements, we estimated property values based on descriptions of the materials. Capillary pressure and relative permeability characteristic curves were approximated for the soil and cobble layers as shown in Table 1 to give a higher capillary pressure in the presumably finer-grained soil than in the cobble for a given liquid saturation. The porosity of both layers was set to 0.35, while the permeabilities of the layers were set to arbitrary values (not shown) to carry out steady-state gravity

capillary equilibrium simulations for which porosity and permeability are not important. Rainfall infiltration was set to zero as the CO_2 releases from the horizontal well were carried out in summer months that tend to have little precipitation. The resulting steady-state static (gravity-capillary equilibrium) moisture profile is shown in Figure 2. Note the capillary barrier (local region of high liquid saturation) that develops in the bottom of the soil layer as a result of stronger capillary pressure in the soil than in the underlying cobble layer in unsaturated conditions (e.g., Oldenburg and Pruess, 1993). The moisture profile of Figure 2 was used as an initial condition for calibrating permeability as described below.

Permeability calibration prior to horizontal well releases

CO_2 injection testing began in October 2006 with CO_2 release from a shallow vertical well to ensure injectivity of the formations present. The shallow vertical-well release consisted of an injection of 1.6 L/min (4.8×10^{-5} kg/s) of CO_2 at a depth of approximately 3 m. Soil CO_2 fluxes (seepage and soil respiration) were measured using an accumulation chamber instrument around the injection well along transects in the N, S, E, and W directions. A 2D radial model with the same soil layers, vertical grid spacing, and moisture distribution as those shown in Figures 1 and 2 for the Cartesian model was used to model this vertical-well injection. Soil CO_2 fluxes measured using an accumulation chamber (Dobeck, unpublished data) were used as constraints to manually fit model permeabilities to the soil and cobble layers. Figure 3 shows the simulated vertical-injection well seepage flux (solid lines) along with the measured data showing the fit obtained for $k_{soil} = 5 \times 10^{-11}$ m^2 (50 Darcy), and $k_{cobble} = 3.2 \times 10^{-12}$ m^2 (3.2 Darcy). The high inferred permeability of the soil likely arises from cracks and root casts that create macropores through which the injected CO_2, soil gas, and atmospheric air are readily transported. Subsequently, these fitted soil and cobble permeabilities were used in forward models using the Cartesian grid (Figure 1) for prediction and

design of the horizontal injection experiment as discussed below. The error arising in this permeability calibration as a result of the coarse vertical grid resolution we used is approximately duplicated in the Cartesian grid making our selection of permeability values consistent between the radial grid and the Cartesian grid. Therefore, we expect the model to have predictive capability for breakthrough time and total flux magnitude. As will be seen in the last section, a much finer grid is needed for resolving the magnitude of molecular diffusion arising from the large concentration gradient at the ground surface.

General description of CO_2 migration

Figure 4 shows model results for four times during simulation of CO_2 injection from the horizontal well with an injection rate of 100 kg d^{-1}. As shown in Figure 4, the CO_2 exits the well directly into the saturated zone (sub-water table) and creates a partially unsaturated CO_2-filled zone around the well. The CO_2 flows upwards by buoyancy and pressure-gradient forces. Note the liquid saturations around the well (solid white lines) after three hours (Figure 4a) are still approximately 90% indicating the gaseous CO_2 is at a saturation of approximately 10%. By a time of one day (Figure 4b), the CO_2 gas has moved into the vadose zone and begins to spread laterally in the cobble layer below the capillary barrier in the soil at ~1 m depth. Spreading in this region of the cobble is favored because of the high intrinsic permeability and lower liquid saturation relative to the soil layer above. Nevertheless, CO_2 penetrates the soil layer after approximately one day and after two days, CO_2 gas has just reached the ground surface (Figure 4c). By this time (two days), the region around the well becomes 20% saturated with gas (gas saturation is equal to one minus the liquid saturation shown by the white contour lines), and lateral spreading in the cobble reaches approximately four meters on each side of the well. After ten days, spreading in the vadose zone

reaches approximately seven meters on each side of the well (Figure 4d). Note the high mass fractions of CO_2 in the gas phase (nearly pure CO_2) consistent with prior results of leakage and seepage modeling (Oldenburg and Unger, 2003). These high soil-gas concentrations produced a steep concentration gradient near the ground surface.

Shown in Figure 5 are results with an injection rate of 1000 kg d^{-1} at times of 3 hours, 1 day, 2 days, and 10 days. The behavior is qualitatively similar to the 100 kg/d injection of Figure 4, but the spreading is larger and the time to breakthrough is shorter.

Fundamental questions pertaining to experiment design

Question 1. What is the time to breakthrough at the surface as a function of injection rate?

The objectives of the experiment included the testing of various CO_2 leakage and seepage detection and monitoring approaches. As such, we wanted the selected injection rates to produce CO_2 leakage and seepage signals that were challenging but not impossible to detect. Also, higher injection rates would be expected to produce surface seepage flux signals of greater magnitude and area that would be advantageous for detection. However, relatively rapid migration of CO_2 in the subsurface associated with relatively high injection rates could make it difficult for researchers to characterize the temporal evolution of the leakage signal and breakthrough at the surface. It was thought an ideal breakthrough time would be longer than a day or two and shorter than a week following the start of injection. With these goals in mind, we simulated various injection rates to aid in the design of the field experiment.

The 100 kg d^{-1} injection rate predicted breakthrough after just under two days whereas the 1000 kg d^{-1} injection predicted breakthrough in less than 12 hours. Figure 6 shows a summary of maximum surface seepage flux and soil CO_2 concentration (12 cm depth) for four different injection rates as a function of time. The predicted smooth breakthrough that occurs after approximately two days for the 100 kg d^{-1} injection rate would allow for the research teams to observe increases in flux (and concentration) from the background measurements before reaching a steady-state seepage condition. Ultimately the team decided to begin the experiment at 100 kg d^{-1} and increase it if either the breakthrough was too slow or the leakage signal could was not detectable by the various methods. As we will show below, neither occurred and the predictive simulation results agreed well with the field measurements.

Question 2: What is the expected pattern of CO_2 discharge at the ground surface?

As shown in Figures 4 and 5, the width of the seepage zone at the ground surface varies with injection flow rate. The 100 kg d^{-1} injection rate produces a zone of anomalous CO_2 flux and concentration with a width of approximately 5 m, while the 1000 kg d^{-1} injection produces a zone of anomalous CO_2 flux and concentration of width approximately 12 m. The maximum seepage fluxes at the ground surface for four different injection rates are shown in Figure 6a and scale closely with the injection rate. The 100 kg d^{-1} rate produced maximum seepage fluxes that appeared to be within the range of detectability for the approaches planned for use (q_{max} ~ 100 μmoles m^{-2} s^{-1} (380 g m^{-2} d^{-1}), approximately 10 times a typical ecological flux). In contrast, the larger injection rates produced fluxes that were larger and likely too easy to detect, at least by some of the approaches being used. The simulations predicted that the flux is largest directly over the well and falls off rapidly on either side of the well. Figure 6b shows the maximum concentrations directly above the well at a depth of

12 cm. These results show again that soil gas concentrations of CO_2 from leakage can become very large even for small fluxes because there are few processes in the shallow subsurface to dissipate leaking CO_2 (e.g., Oldenburg and Unger, 2003). We note that the model is 2D and highly idealized. Local heterogeneity, three-dimensional effects, imperfections in the injection well, and other factors will tend to produce the patchy emission patterns that were ultimately observed in the experiment (Lewicki et al., 2007). Nevertheless, the overall scale of the patches was similar to the width of emission area predicted by these simulations.

Question 3: What is the temporal variation in seepage due to changes in injection rate?

The injection began July 9, 2007 at a rate of 100 kg d^{-1} and lasted for ten days. This period was followed by a shut-in period of 16 days, followed by seven additional days at an injection rate of 300 kg d^{-1}. We present in Figure 7a predictive simulation results for the end of the shut-in period, which follows on effectively from results presented in Figure 4. As shown, the CO_2 has slumped downward in the vadose zone and spread slightly during the shut-in period. Maximum concentrations are still near 100% CO_2 at the well. After one day at an injection rate of 300 kg d^{-1} (Figure 7b), CO_2 rapidly breaks through to the surface. Apparently the new injection lifts the leftover CO_2 in the soil upwards to the surface making the breakthrough time very short. Injection at the higher rate leads to additional lateral spread and higher maximum flux at the ground surface (Figure 7c). We present in Figure 7d a comparison between the time evolution of modeled maximum surface CO_2 fluxes above the well and the CO_2 seepage discharges in tonnes per day (t d^{-1}) estimated by Lewicki et al. (2007) based on accumulation chamber measurements of soil CO_2 flux made on a grid over the injection well. Because there was considerable patchiness in the distribution of measured seepage fluxes at the site, the accumulation chamber measurements are plotted in

Figure 7d as seepage discharges in t d^{-1}, (fluxes integrated over the discharge area above the well). By this means, the areal accumulation chamber data are effectively averaged for comparison to the 2D model results. As shown, the temporal evolution of available measured data match the general trend over time of the predicted surface fluxes. In particular, the predicted rate of increase in seepage flux over time at the start of the first injection, the time to approach steady state during the first injection, and the rapid decline at the end of the second injection agree well with the measurements. For further details on measurement of soil CO_2 fluxes using the accumulation chamber technique, errors associated with these measurements, and data analysis, the reader is referred to Lewicki et al. (2007).

Question 4. What are the dominant transport mechanisms as a function of depth and injection rate?

We used the model to investigate modes of shallow subsurface gas transport during the CO_2 injection tests. We simulated injections of different strengths and compared diffusive to total (advective plus diffusive) transport mechanisms. In other words, we examined the relative strengths of the two terms on the right-hand side of the component flux term giving in Table 1. For these studies, we increased the vertical resolution of the numerical grid in the soil layer by a factor of ten as shown in Figure 8. The higher resolution of the grid is needed to resolve the large CO_2 concentration gradient that exists between ambient air with CO_2 concentration at ~380 ppm (corresponding to CO_2 mass fraction in the aqueous phase equal to 5.76×10^{-4}) and soil gas containing injected CO_2. For this particular study, we injected CO_2 in the model at the bottom of the soil layer at Z = -1.12 m as shown in Figure 8 to avoid the complications of the saturated zone and capillary barrier. For this reason, the resulting model breakthrough times are faster than for the actual horizontal-well injection depth presented above. The molecular diffusion coefficients for all

gas components is set to 10^{-5} m^2 s^{-1} as shown in Table 1. Default multipliers in the model for gas-phase molecular diffusivity dependence on porosity ($\phi = 0.35$), tortuosity of the porous medium ($\tau_0 = 1.0$), and tortuosity arising from saturation ($\tau_\beta = k_{r\beta} = 0.0128$ at $S_g = 0.2$) were used resulting in an effective gas-phase molecular diffusivity for CO_2 of 4.5 x 10^{-8} m^2 s^{-1} at $S_g = 0.2$ (see Pruess et al., 1999, App. D4).

Shown in Figure 9a are comparisons of diffusive and total gas-phase CO_2 transport for three different injection rates where injection occurs at a depth of 1.12 m. As shown, CO_2 injection rates up to approximately 100 kg d^{-1} show transport at the ground surface is primarily by diffusion. Evans et al. (2001) showed through experiments in an instrumented sand bucket apparatus that CO_2 transport at the ground surface is dominated by diffusion even for very large seepage fluxes. The reason that diffusion can dominate transport at high flux of CO_2 is that the concentration gradient becomes very large near the ground surface because the ambient CO_2 concentration in air is fixed at approximately 380 ppm. So while there is still a strong advective component of transport in general, the transport of CO_2 is dominated by diffusion near the ground surface. This allows the use of accumulation chambers that measure mainly diffusive flux to be reasonably accurate surface-CO_2 flux measurement devices, notwithstanding diversion of gas flow when the pressure gradient is high (Evans et al., 2001).

To further elucidate the relative strength of transport processes involved, we present in Figure 9b-d simulation results for gas-phase CO_2 transport mechanisms at three different depths directly above the injection point. As shown in Figure 9b for the lowest injection rate (25 kg d^{-1}), the fluxes at a depth of 0.5 m (Z = -0.5 m) increase first with total flux and diffusive flux nearly equal. Just after

one day, the diffusive flux diminishes while the total flux continues to increase. This occurs because the gradient of CO_2 in the gas phase becomes very small as advection dominates the transport at this location 0.62 m above the injection point. Slightly higher in the soil at Z = -0.10 m, CO_2 transport is 64% by diffusion and 36% by advection, implying the presence of a concentration gradient to sustain diffusion. At the ground surface (Z = -0.02 m), the total CO_2 gas-phase transport is equal to that at Z = -0.10 m, but transport is 91% by diffusion. These results illustrate well the conclusions of Evans et al. (2001) that increased concentration gradient at the ground surface enhances diffusive transport relative to advection even at steady-state conditions.

Figure 9c shows results for an injection rate of 100 kg d^{-1}. As observed for the lower injection rate shown in Figure 9b, there is a short-lived diffusive component of mass transfer at Z = -0.5 m that is quickly overwhelmed by advection as the concentration gradient diminishes. At Z = -0.10 m, the advective transport is 79% of the total transport suggesting smaller concentration gradient in this case than for the 25 kg d^{-1} case. At the ground surface, the diffusive transport is 72% of the total transport. With even greater vertical resolution in the grid in this area, the diffusive component of transport would increase and dominate overall mass transport in the gas phase.

Finally we present in Figure 9d the mass transport at the three depths for an injection rate of 500 kg d^{-1}. In this case, diffusion shows two equal local maxima at early times at both Z = -0.5 m and at Z = -0.10 m as the CO_2 front passes through, demonstrating the importance of advection for this higher injection rate case. At the ground surface, the diffusive transport is 35% of the total transport. Again, with higher vertical resolution, the diffusive component of transport would increase relative

to the advective component because the higher-resolution grid would resolve the vertical concentration gradient more accurately.

These simulations show that transport in the field test when injection rates were 100 kg d^{-1} was mostly by diffusion at the ground surface, but likely mostly advective at depth near the well. When the rate was increased to 300 kg d^{-1} transport was dominated by advection through a larger section of the soil, but transport was still likely mostly diffusive at the ground surface. Our results confirm those of Evans et al. (2001) that at the ground surface, transport of the CO_2 component is primarily diffusive because of the large concentration gradient that exists there. Furthermore these results can be used to constrain measurement and monitoring approaches as a function of depth. Approaches that exploit concentration gradients will be most applicable to very near-surface locations, whereas approaches that can measure advective leakage (e.g., small pressure differences) can be used at greater depths.

Conclusions

Numerical simulations using TOUGH2/EOS7CA informed the key questions (injection rate, breakthrough time, size of seepage zone, transport mechanisms) pertaining to the design of the first set of ZRF CO_2 leakage detection and monitoring experiments. In addition, the modeling provided a greater understanding of likely subsurface flow and transport processes that can be used to design monitoring approaches. First, the permeability calibration using the vertical well release suggests that shallow soils and sediments can be very permeable, e.g., by having cracks and root casts. What this means is that once leaking CO_2 migrates to the shallow subsurface, it will very likely seep out of the ground into the atmosphere in environments like that at the ZRF. Second, the model suggests that the CO_2 transport through the saturated zone is focused and likely occurs by channel flow as the

gas phase displaces water and creates pathways for itself, whereas in the vadose zone CO_2 does not displace water significantly (note liquid saturation contours are largely not perturbed) and spreads out as driven by pressure and density effects.. The model pointed out the importance of the unsaturated region in the cobble layer as an area where migrating CO_2 would tend to spread out laterally. Such regions may be useful areas to target CO_2 concentration monitoring equipment in tests and actual deployments for GCS monitoring. The model suggests that CO_2 concentrations can build up to very high levels even for low injection rates creating a sharp CO_2 concentration gradient near the ground surface, a result already reported in the literature (Oldenburg and Unger, 2003). The modeling also revealed the tendency of the surface flux to fall rapidly when injection stops while concentrations overall in the soil drop slowly, suggesting that high-frequency periodic leakage fluxes, e.g., burping or geysering phenomena originating at depth (e.g., Pruess, 2008), will be manifest in the shallow soil by rapid changes in CO_2 flux. The model results were subsequently validated by comparison to measured seepage rates and showed good agreement. Examination of the transport processes showed that diffusion is more important at shallower depths because the concentration gradient of CO_2 increases as ambient air enters the soil from above. Transport is increasingly dominated by advection closer to the injection point, and as the injection rate increases. Nevertheless at the ground surface, transport of CO_2 appears to be primarily by diffusion justifying the use of the accumulation chamber for measuring surface fluxes. This study demonstrated the utility of TOUGH2/EOS7CA for modeling of shallow CO_2 flow and transport processes.

Acknowledgment

We thank the entire ZERT team for an exciting and supportive research environment. Quanlin Zhou (LBNL) provided helpful internal review comments. This work was carried out in the ZERT project funded by the Assistant Secretary for Fossil Energy, Office of Sequestration, Hydrogen, and Clean Coal Fuels, through the National Energy Technology Laboratory, U.S. Department of Energy under Contract No. DE-AC02-05CH11231.

References

Britter, R.E., Atmospheric dispersion of dense gases, *Ann. Rev. Fluid Mech.*, *21*, 317–344, 1989.

Brooks, M.C., W.R. Zise, M.D. Annable, Fundamental changes in in-situ airsparging flow patterns. *Ground Water Monit. Rem. 19*(2): 105–113, 1999.

Corapcioglu, M.Y., A. Cihan, M. Drazenovic, Rise velocity of an air bubble in porous media: Theoretical studies. *Water Resour. Res. 40*: W04214, 2004.

Cortis, A., C.M. Oldenburg, and S.M. Benson, The role of optimality in characterizing CO_2 seepage from geologic carbon sequestration sites, *Int. J. Greenhouse Gas Control, 2*, 640-652, 2008.

Evans, W.C., M.L. Sorey, B.M. Kennedy, D.A. Stonestrom, J.D. Rogie, and D.L. Shuster, High CO_2 emissions through porous media: transport mechanisms and implications for flux measurement and fractionation, *Chemical Geology 177*, 15-29, 2001.

Hanna, S.R., and K.W. Steinberg, Overview of Petroleum Environmental Research Forum (PERF) Dense Gas Dispersion Modeling Project, *Atmospheric Environment*, *35*, 2223-2229, 2001.

Hillel, D., *Environmental Soil Physics*, Academic Press, San Diego, CA, 771 pp, 1998.

Ji, W., A. Dahmani, D.P. Ahlfied, J.D. Lin, E. Hill III, Laboratory study of air sparging: Air flow visualization, *Ground Water Monit. Rem. 13*(4): 115–126, 1993.

Leuning, R., D. Etheridge, A. Luharb, and B. Dunse, Atmospheric monitoring and verification technologies for CO_2 geosequestration, *Int. J. Greenhouse Gas Control 2*(3), 401-414, 2008.

Lewicki, J.L., C.M. Oldenburg, L. Dobeck, and L. Spangler, Surface CO_2 leakage during the first shallow subsurface CO_2 release experiment, *Geophys. Res. Lett., 34, L24402, 2007.*

Mokwa, R., Subsurface exploration for the MSU CO_2 injection project—Phase I, unpublished report, Montana State University, Civil Engineering Department, 2006.

Oldenburg, C.M., and K. Pruess, On numerical modeling of capillary barriers, *Water Resour. Res.*, *29*(4), 1045–1056, 1993.

Oldenburg, C.M., G.J. Moridis, N. Spycher, and K. Pruess, EOS7C Version 1.0: TOUGH2 Module for Carbon Dioxide or Nitrogen in Natural Gas (Methane) Reservoirs, Lawrence Berkeley National Laboratory Report LBNL-56589, March 2004 (http://www-esd.lbl.gov/TOUGHPLUS/manuals/TOUGH2-EOS7C_Users_Guide.pdf)

Oldenburg, C.M., J.L. Lewicki, and R.P. Hepple, Near-surface monitoring strategies for geologic carbon dioxide storage verification, Lawrence Berkeley National Laboratory Report *LBNL-54089*, October 2003.

Oldenburg, C.M., and J.L. Lewicki, On leakage and seepage of CO_2 from geologic storage sites into surface water, *Env. Geol., 50*(5), 691-705, 2006.

Oldenburg C.M., and A.J.A. Unger, On leakage and seepage from geologic carbon sequestration sites: unsaturated zone attenuation. *Vadose Zone Journal 2*, 287-296, 2003.

Pruess, K. On CO_2 Fluid Flow and Heat Transfer Behavior in the Subsurface, Following Leakage from a Geologic Storage Reservoir, *Env. Geol., 54*(8). 1677–1686, 2008.

Pruess, K., C. Oldenburg, and G. Moridis, *TOUGH2 User's Guide, Version 2.0*, Lawrence Berkeley National Laboratory Report *LBNL-43134*, November 1999.

Pruess, K, ECO2N: A TOUGH2 fluid property module for mixtures of water, NaCl, and CO_2, Lawrence Berkeley National Laboratory Report *LBNL-57952*, August 2005, (http://esd.lbl.gov/TOUGH2/eco2n_man.pdf)

Roosevelt S.E., and M.Y. Corapcioglu, Air bubble migration in a granular porous medium: Experimental studies. *Water Resour. Res. 34*(5): 1131–1142, 1998.

van Genuchten, M.Th, A closed-form equation for predicting the hydraulic conductivity of unsaturated soils, *Soil Sci. Soc., 44*, 892-898, 1980.

Wilkey, P.L, J.E. Bogner, G. Mourad, and T.G. McRae, Rio Vista Gas Leak Study: Belleaire Gas Field, California, *Gas Research Institute GRI-91/0047*, August 1992.

Nomenclature

d	molecular diffusivity	$m^2\ s^{-1}$
g	acceleration of gravity vector	$m\ s^{-2}$
F	Darcy flux vector	$kg\ m^2\ s^{-1}$
k	permeability	m^2
k_r	relative permeability	
M	mass accumulation term	$kg\ m^{-3}$
n	outward unit normal vector	
NK	number of components	
NPH	number of phases	
P	total pressure	Pa
P_c	capillary pressure	Pa
q	mass flux	$kg\ m^{-2}\ s^{-1}$
q_v	volumetric source term	$kg\ m^{-3}\ s^{-1}$
S	saturation.	
t	time	s
T	temperature	^oC
V	volume	m^3
X	mass fraction	
Y	Y-coordinate	
Z	Z-coordinate (positive upward)	

Greek symbols

α	$\rho_w g/P_0$ in van Genuchten's capillary pressure function
β	phase index (subscript)
Γ	surface area m^2
θ	exponent for temperature dependence of diffusivity

κ	mass components (superscript)	
λ	van Genuchten's m	-
μ	dynamic viscosity	kg m^{-1} s^{-1}
ρ	density	kg m^{-3}
τ	tortuosity	
ϕ	porosity	

Subscripts and superscripts

g	gas
l	liquid
s	satiated (saturation)
max	maximum
r	residual
w	water
0	reference value

Tables

Table 1. Governing equations solved in TOUGH2/EOS7CA for isothermal problems.

Description	Equation
Conservation of mass	$\frac{d}{dt}\int_{V_n} M^\kappa dV = \int_{\Gamma_n} \mathbf{F}^\kappa \cdot \mathbf{n} d\Gamma + \int_{V_n} q_v{}^\kappa dV$
Mass accumulation	$M^\kappa = \phi \sum_{\beta=1}^{NPH} S_\beta \rho_\beta X_\beta{}^\kappa$
Phase flux	$\mathbf{F}_\beta = -k \frac{k_{r\beta}\rho_\beta}{\mu_\beta}\left(\nabla P_\beta - \rho_\beta \mathbf{g}\right)$
Component flux	$\mathbf{F}^\kappa = \sum_{\beta=1}^{NPH} \left(X_\beta{}^\kappa \mathbf{F}_\beta - \phi \tau_o \tau_\beta \rho_\beta d_\beta^k \nabla X_\beta{}^\kappa \right)$
Pressure and capillary pressure	$P_\beta = P + P_{c\beta}$
Henry's law	$P_g^\kappa = K_H x_{aq}^\kappa$
Relative permeability (after van Genuchten, 1980)	$if\ S_l < S_{ls},\quad k_{rl} = \sqrt{S^*}\left\{1-\left(1-\left[S^*\right]^{1/\lambda}\right)^\lambda\right\}^2$ $if\ S_l \geq S_{ls} \quad k_{rl} = 1$ $if\ S_{gr} = 0 \quad k_{rg} = 1 - k_{rl}$ $if\ S_{gr} > 0 \quad k_{rg} = \left(1-\hat{S}\right)^2\left(1-\hat{S}^2\right)$ $where\ S^* = \left(S_l - S_{lr}\right)/\left(S_{ls} - S_{lr}\right),$ $\hat{S} = \left(S_l - S_{lr}\right)/\left(1 - S_{lr} - S_{gr}\right)$
Capillary pressure (after van Genuchten, 1980)	$P_c = P_0\left(\left[S^*\right]^{-1/\lambda} - 1\right)^{1-\lambda}$ $subject\ to - P_{\max} \leq P_c \leq 0$
Molecular diffusion	$f_\beta^\kappa = -\phi \tau_o \tau_\beta \rho_\beta d_\beta^k \nabla X_\beta{}^\kappa$ $where\ \tau_o \tau_\beta = \tau_o k_{r\beta}(S_\beta)$ and $d_\beta^k(P,T) = d_\beta^k(P_0,T_0)\frac{P_0}{P}\left[\frac{T+273.15}{273.15}\right]^\theta$

Table 2. Properties of the two layers in the ZRF model.

	Soil	Cobble
Temperature (T)	15 ^{o}C	15 ^{o}C
Porosity (ϕ)	0.35	0.35
Permeability (k)	5 x 10^{-11} m^2	3.2 x 10^{-12} m^2
Capillary Pressure (P_c)	van Genuchten[1,2] λ = 0.291, S_{lr} = 0.15, α = 2.04 x 10^{-4} Pa^{-1}, P_{max} = 5 x 10^5 Pa, S_{ls} = 1.	van Genuchten[1,2] λ = 0.627, S_{lr} = 0.10, α = 1.48 x 10^{-3} Pa^{-1}, P_{max} = 5 x 10^5 Pa, S_{ls} = 1.
Relative permeability (k_r)	van Genuchten[1,2] S_{lr} = 0.17, S_{gr} = 0.05	van Genuchten[1,2] S_{lr} = 0.12, S_{gr} = 0.05
Molec. diffusivity coefficients (d_β^κ)	Liquid: 10^{-10} m^2 s^{-1} Gas: 10^{-5} m^2 s^{-1} θ = 1.0, P_0 = 10^5 Pa	Liquid: 10^{-10} m^2 s^{-1} Gas: 10^{-5} m^2 s^{-1} θ = 1.0, P_0 = 10^5 Pa
Tortuosity (τ_0)	1.0	1.0
Saturation-dependent tortuosity (τ_β)	Equal to relative permeability	Equal to relative permeability

[1]Pruess et al. (1999)

[2]λ is m in van Genuchten's notation.

Figure Captions

Figure 1. Discretization and boundary conditions for the transverse grid.

Figure 2. Initial condition of liquid saturation showing water table at Z = 1.5 m with moisture declining to a minimum at the top of the cobble, with sharp increase in moisture at the bottom of the soil layer (capillary barrier).

Figure 3. Measured soil CO_2 fluxes and their mean at a distance of 1 m from the vertical injection well as a function of time with manually fitted simulation result.

Figure 4. CO_2 mass fraction in the gas (flooded contours) and liquid saturation (white contour lines) at four times for CO_2 injection rate of 100 kg d^{-1} (0.1 t d^{-1}).

Figure 5. CO_2 mass fraction in the gas (flooded contours) and liquid saturation (white lines) at four times for CO_2 injection rate of 1000 kg d^{-1} (1 t d^{-1}).

Figure 6. Summary of simulated CO_2 (a) surface flux and (b) soil gas mass fraction (12 cm depth) evolution above the well for different CO_2 injection rates.

Figure 7. CO_2 mass fraction and liquid saturation (a) after 26 days (16 days of zero injection), (b) after 1 day of injection at 300 kg d^{-1}, (c) after 7 days of injection at 300 kg d^{-1}, and (d) time evolution of predicted maximum CO_2 seepage flux with measured seepage discharge superimposed for validation.

Figure 8. Fine mesh for studying diffusive and advective gas-phase CO_2 transport near the ground surface from release at the point labeled “Injection point.”

Figure 9. (a) Time evolution of the total (advection plus diffusion) and diffusive components of CO_2 mass transport directly above the well for injection at different rates into the bottom of the soil layer calculated using the fine mesh. (b) Evolution of the total and diffusive components of CO_2 transport for injection rate of 25 kg d^{-1} at depths of Z = -0.5, -0.1, and -0.02 m vertically above the injection point. (c) Evolution of the total and diffusive components of CO_2 transport for injection rate of 100 kg d^{-1} at the same three depths in the system. (d) Evolution of the total and diffusive components of CO_2 transport for injection rate of 500 kg d^{-1} at the same three depths in the system.

Figures

Figure 1

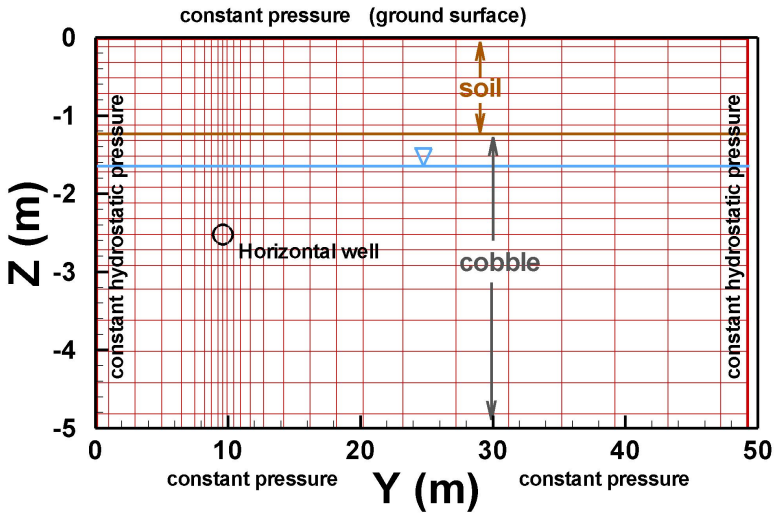

Figure 2

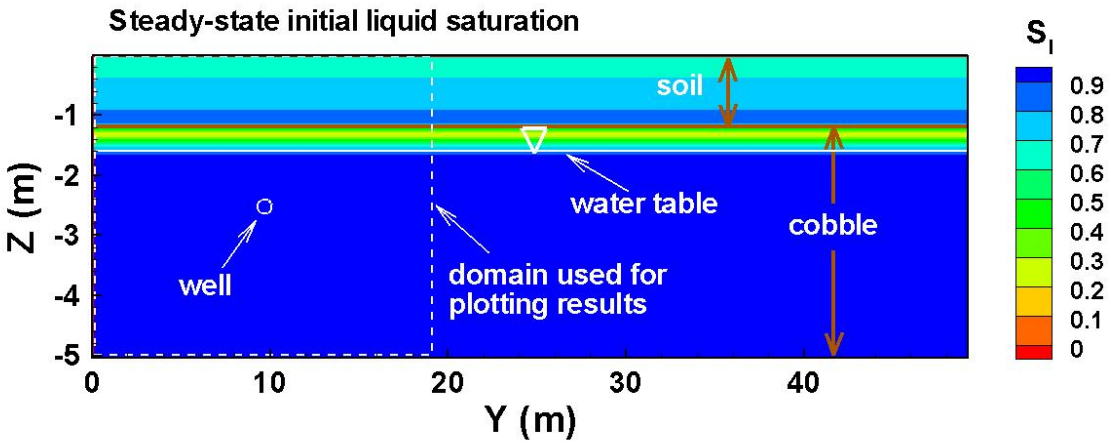
Steady-state initial liquid saturation
soil
water table
cobble
well
domain used for
plotting results
Z (m)
-1
-2
-3
-4
-5
0
10
20
30
40
Y (m)
S_l
0.9
0.8
0.7
0.6
0.5
0.4
0.3
0.2
0.1
0

Figure 3

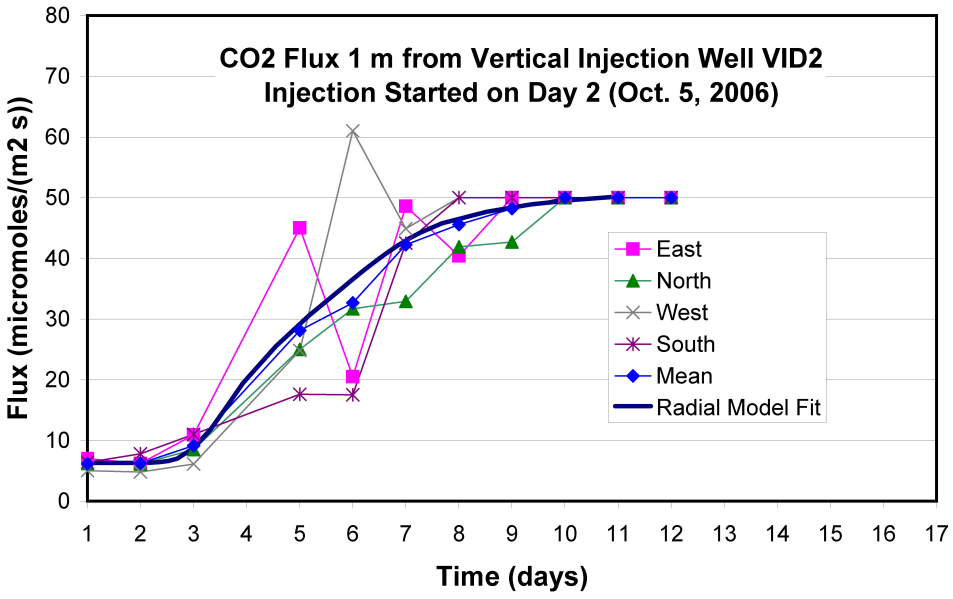
CO2 Flux 1 m from Vertical Injection Well VID2
Injection Started on Day 2 (Oct. 5, 2006)
Flux (micromoles/(m2 s))
Time (days)
East
North
West
South
Mean
Radial Model Fit
0
10
20
30
40
50
60
70
80
1
2
3
4
5
6
7
8
9
10
11
12
13
14
15
16
17

Figure 4

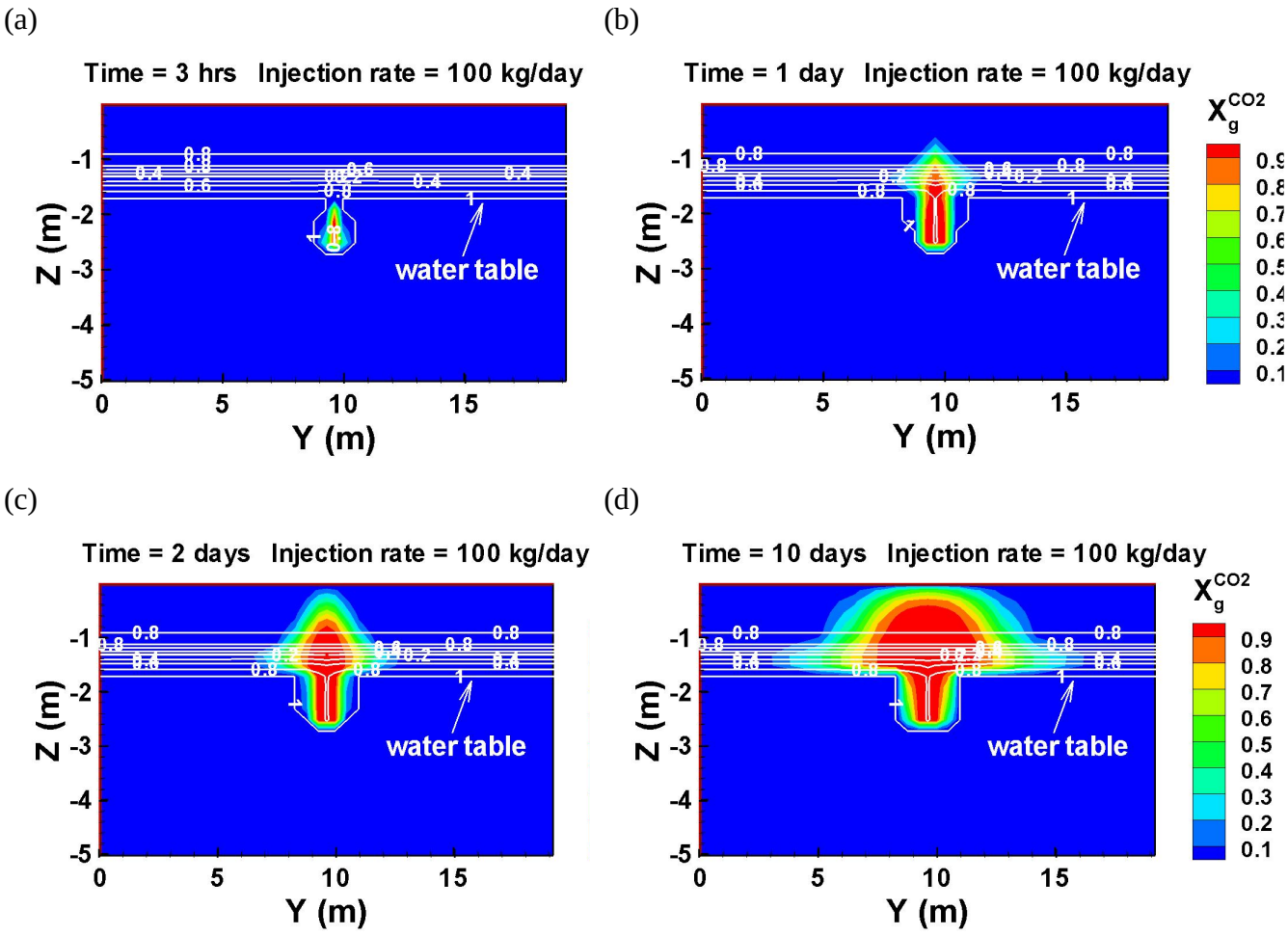
(a)
Time = 3 hrs Injection rate = 100 kg/day
water table
Z (m)
Y (m)
(b)
Time = 1 day Injection rate = 100 kg/day
water table
Z (m)
Y (m)
X_g^{CO2}
(c)
Time = 2 days Injection rate = 100 kg/day
water table
Z (m)
Y (m)
(d)
Time = 10 days Injection rate = 100 kg/day
water table
Z (m)
Y (m)
X_g^{CO2}

Figure 5

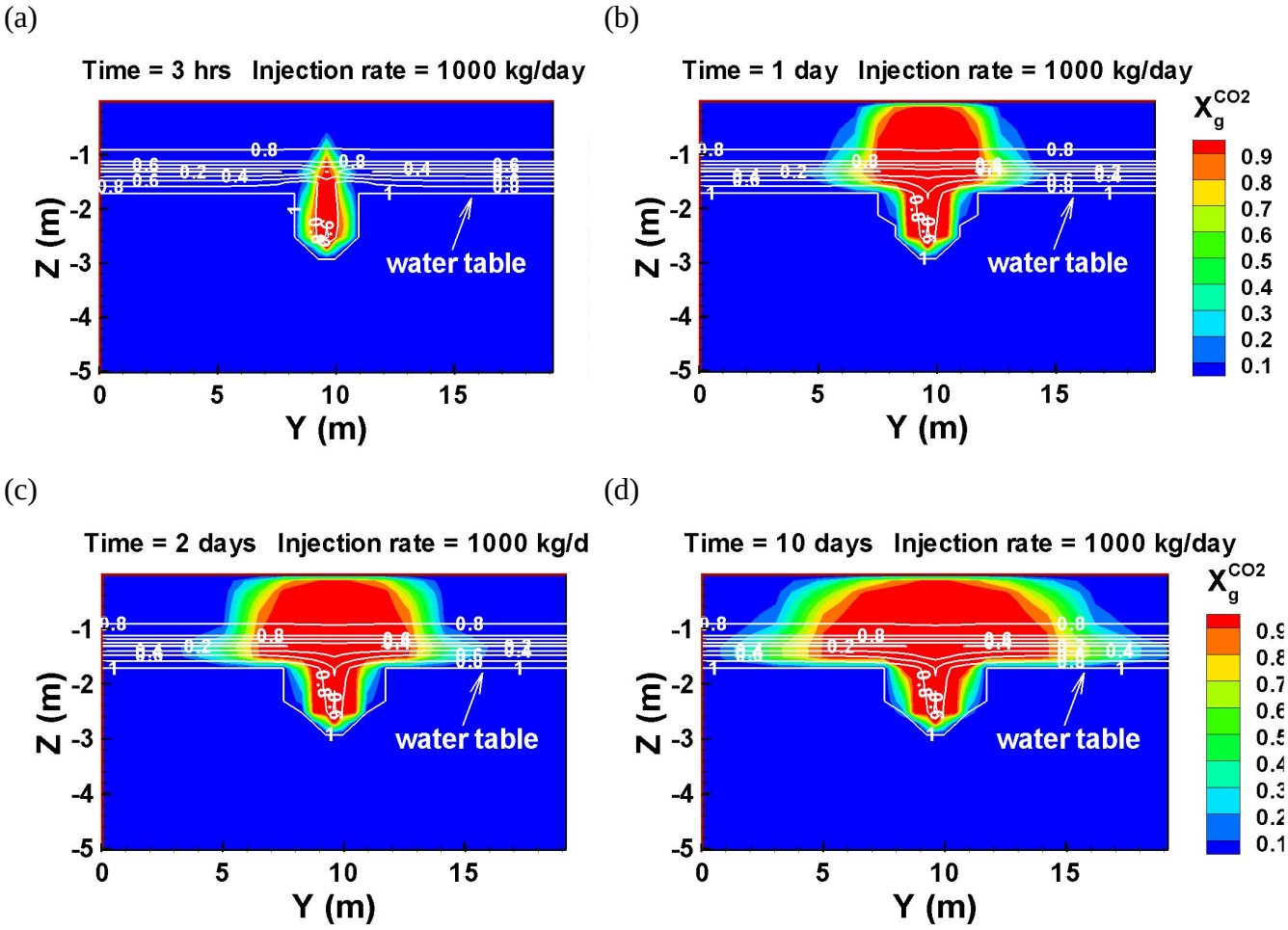
(a)
Time = 3 hrs Injection rate = 1000 kg/day
(b)
Time = 1 day Injection rate = 1000 kg/day
(c)
Time = 2 days Injection rate = 1000 kg/d
(d)
Time = 10 days Injection rate = 1000 kg/day
water table
Z (m)
Y (m)
X_g^{CO2}
0.9
0.8
0.7
0.6
0.5
0.4
0.3
0.2
0.1

Figure 6

(a)

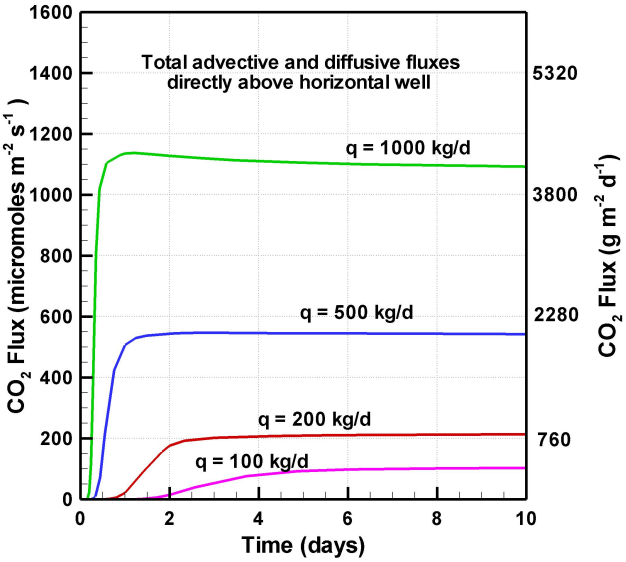
Total advective and diffusive fluxes
directly above horizontal well
q = 1000 kg/d
q = 500 kg/d
q = 200 kg/d
q = 100 kg/d
CO2 Flux (micromoles m-2 s-1)
CO2 Flux (g m-2 d-1)
Time (days)
0
200
400
600
800
1000
1200
1400
1600
760
2280
3800
5320
0
2
4
6
8
10

(b)

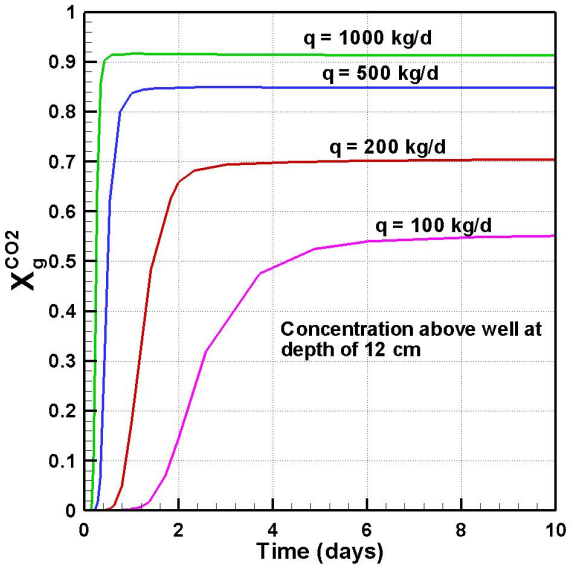
q = 1000 kg/d
q = 500 kg/d
q = 200 kg/d
q = 100 kg/d
Concentration above well at
depth of 12 cm
Xg CO2
Time (days)
0
0.1
0.2
0.3
0.4
0.5
0.6
0.7
0.8
0.9
1
0
2
4
6
8
10

Figure 7

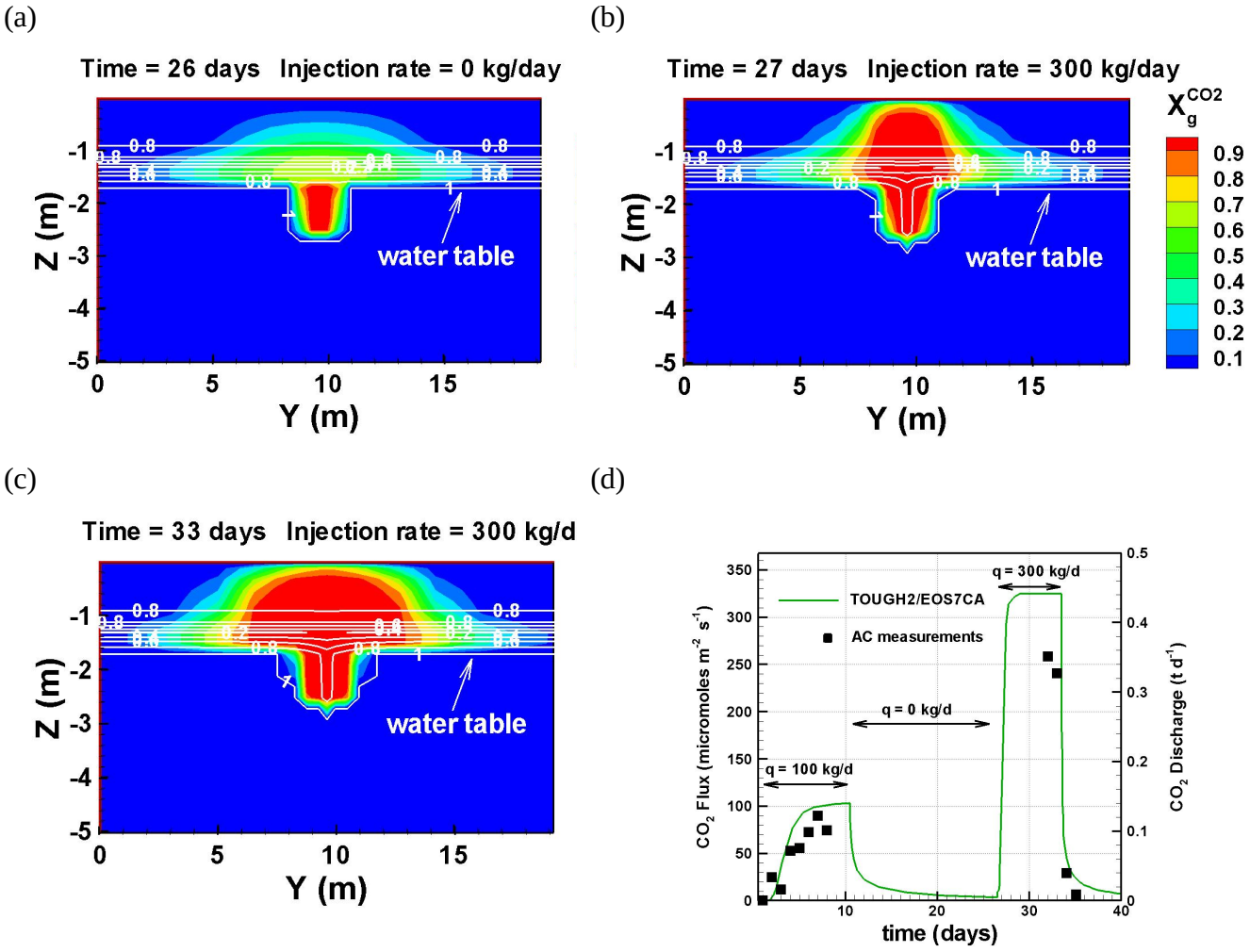
(a)
Time = 26 days Injection rate = 0 kg/day
water table
Z (m)
Y (m)
(b)
Time = 27 days Injection rate = 300 kg/day
water table
X_g^{CO2}
0.9
0.8
0.7
0.6
0.5
0.4
0.3
0.2
0.1
Z (m)
Y (m)
(c)
Time = 33 days Injection rate = 300 kg/d
water table
Z (m)
Y (m)
(d)
TOUGH2/EOS7CA
AC measurements
q = 300 kg/d
q = 0 kg/d
q = 100 kg/d
CO_2 Flux (micromoles m^{-2} s^{-1})
CO_2 Discharge (t d^{-1})
time (days)

Figure 8

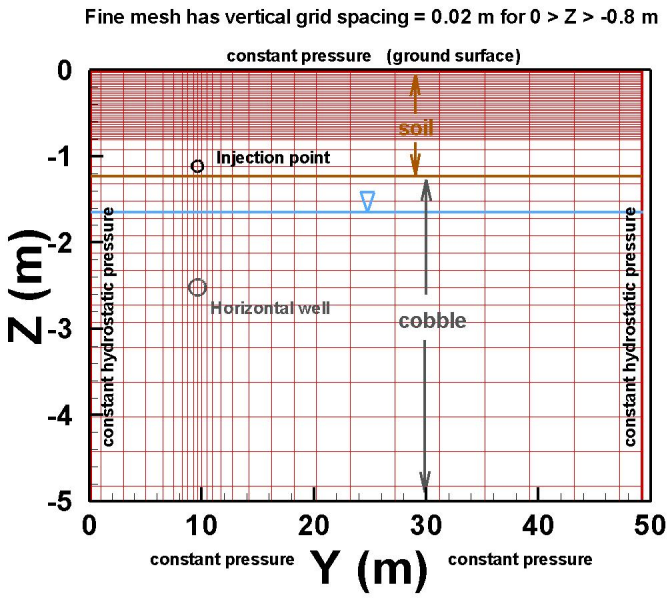
Fine mesh has vertical grid spacing = 0.02 m for 0 > Z > -0.8 m
constant pressure (ground surface)
soil
Injection point
Horizontal well
cobble
constant hydrostatic pressure
constant hydrostatic pressure
constant pressure
constant pressure
Z (m)
Y (m)
0
-1
-2
-3
-4
-5
0
10
20
30
40
50

Figure 9

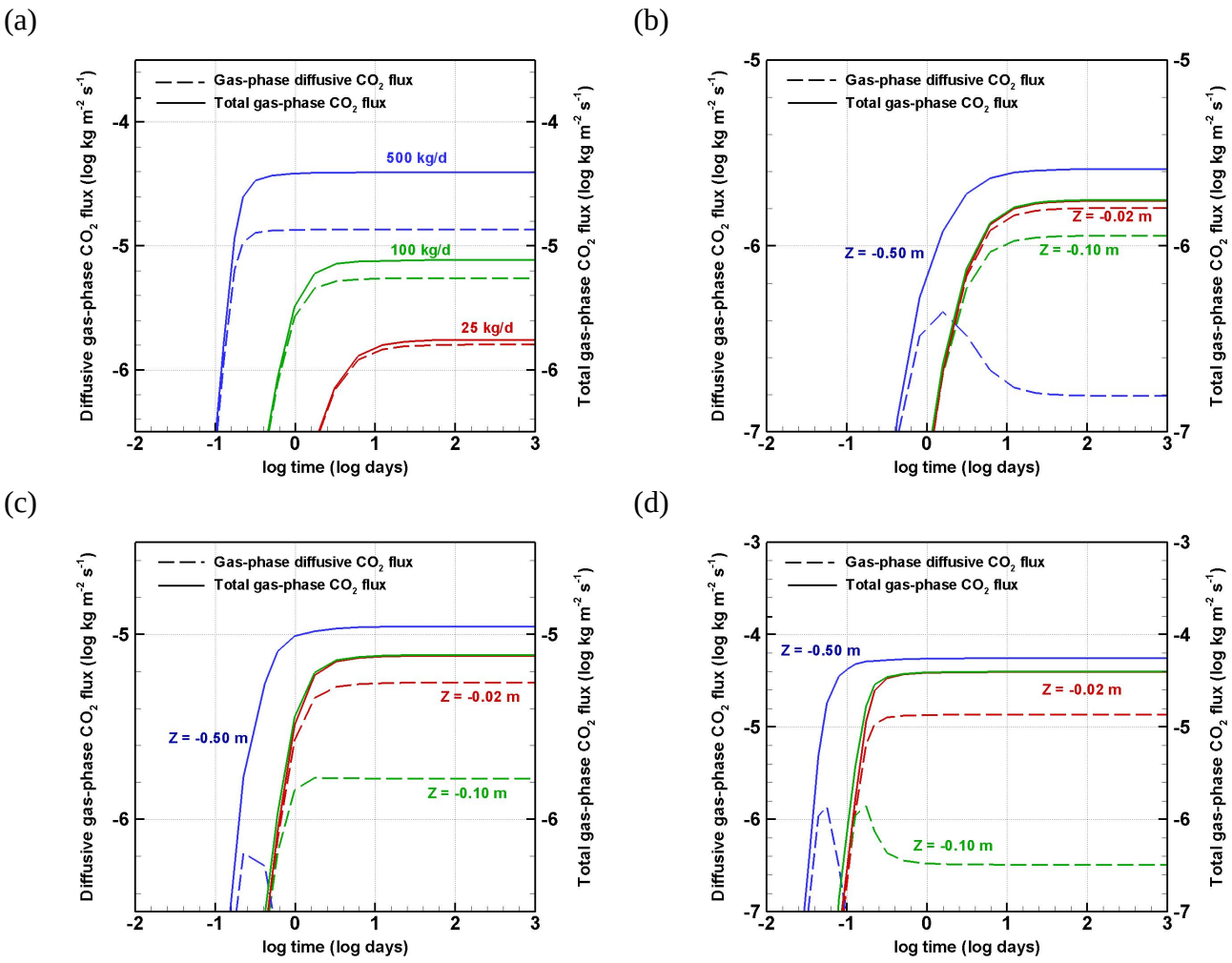
(a)
(b)
(c)
(d)
Gas-phase diffusive CO_2 flux
Total gas-phase CO_2 flux
Diffusive gas-phase CO_2 flux (log kg m^{-2} s^{-1})
Total gas-phase CO_2 flux (log kg m^{-2} s^{-1})
log time (log days)
500 kg/d
100 kg/d
25 kg/d
Z = -0.50 m
Z = -0.02 m
Z = -0.10 m